Thallium Adsorption onto Illite

Silvan Wick,[†,‡] Bart Baeyens,[§] Maria Marques Fernandes,[§] and Andreas Voegelin*[†]

[†]Eawag, Swiss Federal Institute of Aquatic Science and Technology, Überlandstrasse 133, CH-8600 Dübendorf, Switzerland
[‡]Institute of Biogeochemistry and Pollutant Dynamics, ETH Zürich, CH-8092 Zürich, Switzerland
[§]Paul Scherrer Institute, CH-5232 Villigen PSI, Switzerland

Ⓢ *Supporting Information*

ABSTRACT: We investigated the adsorption of Tl^+ onto purified Illite du Puy (IdP). Distribution coefficients (K_d) for trace Tl adsorption indicated a moderate pH-dependence from pH 2.5 to 11. Adsorption isotherms measured at Tl^+ concentrations from 10^{-9} to 10^{-2} M at near-neutral pH on illite saturated with Na^+ (100 mM), K^+ (1 and 10 mM), NH_4^+ (10 mM) or Ca^{2+} (5 mM) revealed a high adsorption affinity of Tl^+ in Na^+- and Ca^{2+}-electrolytes and strong competition with K^+ and NH_4^+. Cation exchange selectivity coefficients for Tl^+ with respect to Na^+, K^+, NH_4^+, and Ca^{2+} were derived using a 3-site sorption model. They confirmed the strong adsorption of Tl^+ at the frayed edges of illite, with Tl selectivity coefficients between those reported for Rb^+ and Cs^+. X-ray absorption spectra of Tl adsorbed onto Na-exchanged IdP indicated a shift from adsorption of (dehydrated) Tl^+ at the frayed edges at low loadings to adsorption of (hydrated) Tl^+ on planar sites at the highest loadings. Our results suggest that illite is an important adsorbent for Tl in soils and sediments, considering its often high abundance and its stability relative to other potential adsorbents and the selective nature of Tl^+ uptake by illite.
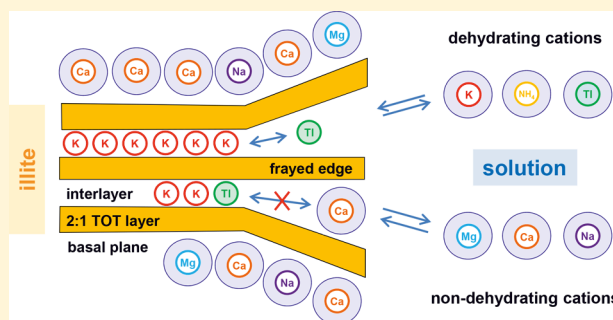
INTRODUCTION

Thallium (Tl) is a highly toxic trace element. It occurs in the environment predominantly as monovalent Tl^I and to a lesser extent as trivalent Tl^{III}.[1,2] Since the ionic radius of Tl^+ (1.70 Å for 12-fold coordination) is similar to the ionic radius of K^+ (1.64 Å),[3] Tl^I can substitute K^+ in K-bearing rock-forming minerals such as K-feldspars or micas,[1,4,5] but is also found in rare minerals such as dorallcharite $(Tl_{0.8}K_{0.2}Fe_3(SO_4)_2(OH)_6)$[6] and lanmuchangite $(TlAl(SO_4)_2·12H_2O)$.[7] Tl^{III} occurs in water as strongly hydrolyzing aqua cation Tl^{3+},[1] forms poorly soluble avicennite (Tl_2O_3)[8] and can be stabilized in Mn-oxides.[9,10]

Typical Tl contents in soils and sediments range between 0.1 and 1 mg/kg.[11] High geogenic Tl contents of up to several thousand mg/kg may be found in soils formed on rocks hosting Tl-rich mineralizations.[12,13] Anthropogenic Tl contamination can result from cement production,[14] metal mining and smelting[15,16] or coal burning.[2,17] Because Tl^+ is relatively soluble, it may be leached into the groundwater or taken up by plants and, via the food chain, may also pose a threat for human health.[18,19] In soils and sediments, the solubility of Tl is controlled by the stability of Tl-bearing minerals and adsorption processes. Based on the geochemical association of Tl with micas and Mn-oxides,[4,5,20] micaceous phyllosilicates such as illite and the phyllomanganate birnessite have long been assumed to be key adsorbents for Tl in soils and sediments.[1,4,16,21−24] This assumption has been corroborated by a recent spectroscopic study on the speciation of Tl in a geogenically Tl-rich soil, which documented the occurrence of Tl^{III} in soil Mn-concretions and confirmed the importance of Tl^I sequestration by illite.[12]

Illite is a 2:1 type clay mineral with a basal spacing of 10 Å whose layers are held together by dehydrated K^+ in the interlayers. Illite in soils may form by the weathering of muscovite or may be inherited from sedimentary parent material.[25] Replacement of K^+ at the edges of illite by larger and strongly hydrated cations like Ca^{2+} leads to an expansion of the interlayer spacing to 14 Å within the so-called frayed edge zone.[26,27] The frayed edges of illite are known to have a very high adsorption selectivity for the weakly hydrated alkali metal cations K^+, Rb^+, and Cs^+ and for NH_4^+. The adsorption of these cations onto illite has been extensively studied with respect to the availability of the nutrients K^+ and NH_4^+[28,29] and the retention of the radionuclide ^{137}Cs in soils contaminated from nuclear accidents or in potential host rocks for radioactive waste storage.[25,26,29−33] To describe the adsorption of Cs^+ by illite in the presence of competing cations, a multi-site cation exchange model was developed by Brouwer et al. (1983)[34] and generalized by Bradbury and Baeyens (2000)[35] based on three types of cation exchange sites: (i) frayed edge sites (FES) with a very low adsorption capacity (0.25% of the cation exchange capacity (CEC) of illite) but very high affinity, (ii) type-II sites

(T2S) with an intermediate affinity and relatively high adsorption capacity (20% of CEC) and (iii) planar sites (PS) on the basal surfaces of illite with a low limited selectivity but high capacity (~80% of CEC). Over time, cations adsorbed to FES can diffuse into the interlayer and replace K^+, leading to their fixation in the illite structure, as observed for Cs^+.[26]

Because of the similarities in dehydration energy and ionic radius between Tl^+ and K^+ and the occurrence of elevated concentrations of Tl in K-rich minerals including micas, Tl has been postulated to be effectively taken up by illite (or, more generally, micaceous clay minerals) in soils and sediments.[1,4,12,16,21−24,36] However, the adsorption of Tl^+ by illite has not been studied to date and cation exchange selectivity coefficients are lacking. In this study, we therefore investigated the cation exchange selectivity of Tl^+ on purified homoionic Na-, K-, NH_4-, and Ca-illite. We determined the pH-dependence of Tl^+ adsorption at trace concentration and the concentration-dependence at near-neutral pH. From the adsorption isotherms, cation exchange selectivity coefficients were derived based on the generalized 3-site Cs^+ sorption model for illite. X-ray near edge structure (XANES) spectra at the Tl L_{III}-edge were collected on Na-illite with different Tl^+ loadings to gain insight into the mechanism of Tl^+ uptake.

■ MATERIALS AND METHODS

Illite du Puy. The illite used for this work has been collected near Le Puy-en-Velay (France) and has previously been used in adsorption studies with different trace metals.[37−39] Purified and conditioned Illite du Puy (IdP) suspensions used for the present work were prepared from the same illite source material and following the same procedure as described in detail in previous work.[37] In a first step, IdP was conditioned to homoionic Na^+ form (100 mM NaCl). Using the dialysis technique,[37] initial Na-IdP suspensions were brought to Na^+, K^+, NH_4^+ and Ca^{2+} forms with different background electrolyte concentrations: Na-IdP (in 100 mM $NaNO_3$), K-IdP (in 1 and 10 mM KNO_3), Ca-IdP (in 5 mM $Ca(NO_3)_2$) and NH_4-IdP (in 10 mM NH_4NO_3).

The purified IdP has been reported to mineralogically consist of 88% illite and 12% sanidine.[37] The small sanidine fraction was considered to be nonreactive with respect to Tl^+ adsorption. A N_2-BET surface area of 103 m^2/g has been determined for purified IdP used in this study, in good agreement with a reported N_2-BET surface area of 97 m^2/g.[37] The elemental composition of the purified IdP (48.4% SiO_2, 20.4% Al_2O_3, 7.6% Fe_2O_3, 6.7% K_2O, 3.9% MgO, 0.1% CaO and 0.9% Na_2O) conforms with the compositional formula $[Si_{6.98}Al_{1.02}O_{20}(OH)_4][Al_{2.44}Fe^{III}_{0.82}Mg_{0.84}][Ca_{0.02}Na_{0.24}K_{1.24}]$ proposed by Poinssot et al. (1999)[40] for another batch of Illite du Puy and with the description of Illite du Puy given by van Olphen and Fripiat (1979).[41] Using the Cs isotope dilution technique[42] with ^{204}Tl instead of ^{137}Cs, a Tl-CEC of 0.260 eq/kg was determined for one of the purified IdP batches used in this study, in excellent agreement with the Cs-CEC of 0.263 eq/kg of the respective batch.

General Setup of Adsorption Experiments. Batch adsorption experiments with homoionic IdP suspensions were conducted as a function of solution pH and Tl concentration in different background electrolyte (see SI Table S1 for an overview of the experimental conditions). All experiments were carried out in 40 mL polypropylene centrifuge tubes (Beckman Coulter). Stable $^{203/205}Tl$ stock

solutions were prepared from $TlNO_3$ in the required background electrolyte and were labeled with radioactive ^{204}Tl (β-emitter; $T_{1/2}$ = 3.78 years; provided by RC TRITEC AG (Teufen, Switzerland); ICP-MS analysis of the tracer solution (0.6 MBq/g): 3.7% ^{204}Tl, 94.3% ^{203}Tl and 2% ^{205}Tl). The background electrolyte was spiked with the desired total Tl concentration, and the pH of the solution was adjusted by either HNO_3 or NaOH additions or by using organic pH buffers. Homoionic IdP suspensions were added to obtain the optimal final adsorbent concentrations, depending on the expected extent of Tl uptake. Subsequently, the tubes were closed and shaken end-overend at room temperature. Based on preliminary experiments on the kinetics of Tl^+ uptake by IdP (details in Supporting Information; Figure S1), a reaction time of 14 days was used for the experiments described below. After reaction, phase separation was carried out by ultracentrifugation (1 h at 108,000 g (max), Beckman Coulter Avanti J30i High-Performance Centrifuge). Two 5 mL aliquots of the supernatant were radio-assayed for the remaining ^{204}Tl activity using a liquid scintillation counter (Packard Tri-Carb 2750 TRILL) and the average of these two independent determinations of remaining activity was taken as one experimental data point. The pH was measured immediately after phase separation in the remaining supernatant. From the decrease in ^{204}Tl activity and the known total Tl concentration ($C_{Tl,init}$, [mol/L]), the final dissolved Tl concentration in the supernatant (C_{Tl}, [mol/L]) was derived. From the decrease in dissolved Tl during reaction, the suspension volume (V_{batch}, [L]) and the mass of illite (m_{IdP}, [kg]), the amount of adsorbed Tl (Q_{Tl}, [mol/kg]) was obtained. Distribution coefficients K_d (in [L/kg]) describing the ratio between dissolved Tl and adsorbed Tl were calculated according to eq 1:

$$K_d = \frac{Q_{Tl}}{C_{Tl}} = \frac{(C_{Tl,init} - C_{Tl})}{C_{Tl}} \times \frac{V_{batch}}{m_{IdP}} \quad (1)$$

Each experiment was run in duplicate and the values were treated as independent data points.

pH-Dependent Adsorption. pH adsorption edges were measured on Na-IdP (100 mM NaCl) and K-IdP (10 and 100 mM KNO_3) in the pH range from ~2.5 to ~11.0. Total initial Tl concentration, that is, carrier $^{203/205}Tl$ and tracer ^{204}Tl, was 10^{-8} M. First, the Tl solution was added to the 40 mL centrifuge tubes. Subsequently, the pH was adjusted by either adding 0.1 M HNO_3 (Merck Titrisol, for pH 4.0 to 5.0), 1 M HNO_3 (Merck Titrisol, for pH 2.5−3.9), 0.1 M NaOH (Merck Titrisol, for pH 10.0−11.0) or 5 mL of prepepared organic buffer solutions (for pH 5.3 to 6.8: 0.015 M MES (2-(N-morpholino)ethanesulfonic acid); for pH 6.9 to 7.8: 0.015 M MOPS (3-(N-morpholino)propanesulfonic acid); for pH 7.9 to 8.6: 0.015 M TRIS (Tris(hydroxymethyl)aminomethane); for pH 8.7 to 9.9: 0.015 M CHES (2-(cyclohexylamino)-ethanesulfonic acid)). Finally, the IdP-suspension was added to achieve an IdP concentration of 2 g/L.

Concentration-Dependent Adsorption. Adsorption isotherms were measured on Na-IdP (100 mM NaCl (low Tl concentrations) or $NaNO_3$ (high Tl concentrations; to avoid precipitation of TlCl)), K-IdP (1 and 10 mM KNO_3), Ca-IdP (5 mM $Ca(NO_3)_2$) and NH_4-IdP (10 mM NH_4NO_3) for total Tl concentrations from 10^{-9} to 10^{-2} M. The solutions with different Tl concentrations were obtained by diluting a 10^{-2} M $TlNO_3$ stock solution to different levels. The resulting

solutions were labeled separately with [204]Tl. The pH of each Tl solution was adjusted to ~7.0 using 0.1 M NaOH or 0.1 M HNO$_3$ (both Merck Titrisol). The solutions were pipetted in the 40 mL centrifuge tubes, followed by the addition of IdP-suspension to obtain an IdP concentration of 0.7 to 3.8 g/L. Final pH values after equilibration ranged between 6.1 and 6.9 (see Supporting Information (SI) Table S1).

Adsorption Modeling. All adsorption isotherm data (5 isotherms; 230 data points) were used to derive cation exchange selectivity coefficients for Tl$^+$-Na$^+$, Tl$^+$-K$^+$, Tl$^+$-NH$_4$$^+$, and Tl$^+$-Ca^{2+} exchange based on the generalized 3-site cation exchange model for Cs$^+$ adsorption onto illite of Bradbury and Baeyens (2000),[35] that is, based on the respective site types and fractions. Cation exchange was treated according to the convention of Gaines and Thomas (1953)[43] (i.e., assuming the activity of adsorbed cations to correspond to their equivalent charge fraction, eqs 2−4):

$$A^{n+} + \frac{n}{m}BX_m = AX_n + B^{m+} \tag{2}$$

$$K_A^B = \frac{(a_{A^{n+}})^m \times (N_{BX_m})^n}{(N_{AX_n})^m \times (a_{B^{m+}})^n} \tag{3}$$

$$N_{AX_n} = \frac{n \times Q_{AX_n}}{Q_{tot,X}} N_{BX_m} = \frac{m \times Q_{BX_m}}{Q_{tot,X}} \tag{4}$$

where A and B represent cations with charges n and m respectively, AX_n and BX_m the respective cations bound to the exchange site(s) X, K_A^B the cation exchange selectivity coefficient, a_{An+} and a_{Bm+} the activity of the free cations in solution (in [mol/L]), N_A and N_B the equivalent fractions of the exchangeable bound cations, Q_{AXn} and Q_{BXm} the amounts of the cations A or B bound to site X (in [mol/kg]) and $Q_{tot,X}$ the total concentration of site X (in [eq/kg]; X representing FES, T2S, and PS).

The model was implemented in the geochemical equilibrium code PhreeqC using the thermodynamic database Minteq V4 and the Davies equation for the calculation of activity coefficients.[44] For Tl^I, only the stability constants of the aqueous complexes TlCl, TlCl$_2$$^-$, and TlNO$_3$ were included; oxidation of Tl^I to Tl^{III} and precipitation of Tl-bearing phases were excluded. Similarly, only NH$_4$$^+$ and NH$_3$ were included as dissolved N^{-III} species, and oxidation of N^{-III}, formation of any solution complexes or precipitation of solids was excluded. For parameter refinement, the PhreeqC model was set up in the software code PhreePlot,[45] using the nonlinear least-squares (modified Levenberg−Marquardt) algorithm to obtain optimized parameters and their uncertainty. For parameter refinement, the sum of the squared residuals between experimental and calculated log K_d values was minimized, based on the total concentrations of Tl$^+$, Na$^+$, K$^+$, NH$_4$$^+$, Ca^{2+}, Cl$^-$, and NO$_3$$^-$ and the mass of homoionic illite in the suspensions. The fractions of FES (0.25% of CEC), T2S (20% of CEC), and PS (79.75% of CEC) on illite from the generalized 3-site Cs$^+$ sorption model,[35] and the experimental Tl-CEC (0.260 eq/kg) were used to calculate the individual site capacities, which were treated as nonadjustable parameters in the model ($Q_{tot,FES}$ = 0.00065 eq/kg; $Q_{tot,T2S}$ = 0.05200 eq/kg; $Q_{tot,PS}$ = 0.20735 eq/kg).

Tl L$_{III}$-Edge XANES Spectroscopy. For XANES analyses at the Tl L$_{III}$-edge, Tl was adsorbed to Na-IdP at Tl loadings from 2.5 × 10^{-4} to 2.4 × 10^{-1} mol/kg (50 to 49'000 mg/kg) at

background NaCl concentrations of 100 mM (2.5 × 10^{-4} to 1.9 × 10^{-2} mol/kg), 95 mM (5.9 × 10^{-2} mol/kg) or 12 mM (2.4 × 10^{-1} mol/kg). After the 14-days reaction time, the Tl loaded illite was separated by ultracentrifugation and supernatant was decanted. The resulting wet paste was filled in acrylic glass sample holders covered with Kapton tape. Based on a water content of the illite pastes of ~50% (by weight; after centrifugation), dissolved Tl was estimated to correspond to ~3% of the total Tl in the most concentrated sample and to be insignificant in all other samples. A reference spectrum was collected on a 10 mM TlNO$_3$ solution. The XANES spectra were recorded at the SuperXAS beamline (Swiss Light Source, PSI, Switzerland) at room temperature in fluorescence mode using a 5-element silicon drift detector. For data extraction and analysis, the software code Athena was used.[46]

RESULTS AND DISCUSSION

Trace Tl$^+$ Adsorption from pH ~2.5 to ~11.0. Distribution coefficients (K_d) for trace Tl$^+$ adsorption from pH ~ 2.5 to ~11.0 in 100 mM NaCl, 10 mM and 100 mM KNO$_3$ background electrolyte are shown in Figure 1A. From 100 mM Na$^+$ to 10 mM K$^+$ electrolyte, a pronounced decrease in K_d values by about 1.5 log units can be observed over the entire pH range, indicating that K$^+$ much more strongly interferes with trace Tl$^+$ uptake than Na$^+$. K_d values further decrease by about one order of magnitude when the K$^+$ concentration increases from 10 to 100 mM. The constant decrease of the log K_d values over the probed pH range when the background electrolyte was varied from 100 mM Na$^+$ over 10 mM K$^+$ to 100 mM K$^+$ clearly points to cation exchange as the dominant adsorption process over the probed pH range. The data further suggested that oxidation of Tl$^+$ to poorly soluble or strongly binding Tl^{3+} did not detectably contribute to Tl removal from solution, since both Tl$^+$ oxidation and Tl^{3+} precipitation or adsorption would strongly depend on solution pH rather than the type or concentration of the background electrolyte cation.

From pH ~2.5 to ~11.0, K_d values in all three background electrolytes increased regularly by up to 1.3 log units. In the acidic region a smooth gradual decrease of the log K_d with decreasing pH cannot be explained by proton competition on exchange sites alone, because proton competition is only relevant at pH values ≤4 and would lead to a steep decrease in log K_d with further decreasing pH (as seen in model calculations for pH-dependent Cs$^+$ uptake by illite).[40] Specific adsorption of Tl$^+$ at the variably protonated surface hydroxyl groups at the broken bond and edge sites (not FES) of illite platelets could contribute to the more pronounced increase of the adsorption affinity of Tl$^+$ at alkaline pH.[37] Based on the relationship between the hydrolysis constants of metal cations and their adsorption constants for coordination at illite edge sites reported in previous work[37,47] and considering the pK$_1$ of Tl$^+$ of 13.2, adsorption of Tl$^+$ onto these sites is expected to be weak at acidic to slightly alkaline pH values, but could become relevant at pH >10. Other factors that may contribute to increasing log K_d values with increasing pH could include changes in illite surface charge and structure. Finally, illite dissolution at acidic and alkaline pH could affect Tl adsorption, but was expected to be of minor relevance, considering that only 0.1% Illite du Puy has been reported to dissolve within 7 days at pH 3.0[40] and that dissolution rates at pH 4−10 are lower than at pH 3.[48] Although the processes responsible for the observed pH-dependence of Tl$^+$ adsorption could not be
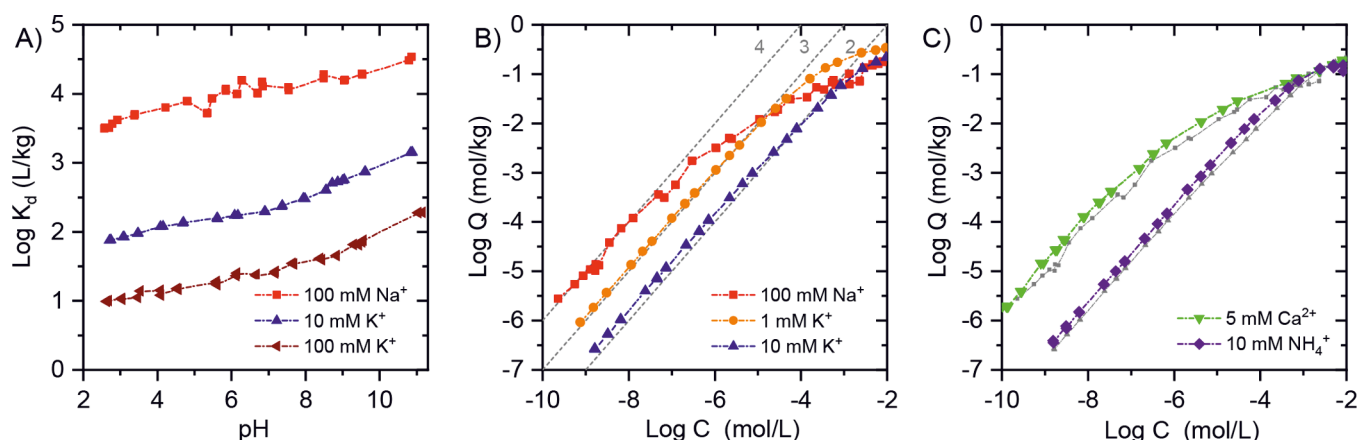
Figure 1. (A) Log K_d of trace Tl$^+$ adsorbed onto Na-illite (100 mM NaCl) and K-illite (10 and 100 mM KNO$_3$) from pH ~2.5 to ~11.0. (B) Adsorption isotherms for Tl$^+$ on illite at near neutral pH in 100 mM NaCl or NaNO$_3$, 1 mM and 10 mM KNO$_3$ electrolyte (diagonal gray dashed lines represent log K_d values of 4, 3, and 2 L/kg). (C) Adsorption isotherms for Tl$^+$ on illite at near neutral pH in 5 mM Ca(NO$_3$)$_2$ and 10 mM NH$_4$NO$_3$. Data for 100 mM Na$^+$ and 10 mM K$^+$ from panel B are shown in gray for comparison.

identified in this study, it is important to note that the log K_d values in all three electrolytes vary by only ~0.3 from pH 6 to 8, that is, that the pH-dependence of Tl$^+$ adsorption onto illite at near neutral pH is weak.

Tl$^+$ Adsorption Isotherms in Different Background Electrolytes. In Figure 1B, the adsorption isotherms of Tl$^+$ onto Na-IdP (100 mM NaCl or NaNO$_3$) and K-IdP (1 and 10 mM KNO$_3$) are shown. The comparison of the adsorption isotherms in 100 mM Na$^+$ and in 10 mM K$^+$ clearly demonstrate that K$^+$ effectively reduces Tl$^+$ uptake at low Tl concentrations ($<10^{-4}$ M) where specific uptake mechanisms are expected to prevail (Figure 1B). Only at the highest dissolved Tl concentrations, where cation exchange is expected to take place on PS, log K_d values in the presence of 100 mM Na$^+$ are lower than in the presence of 10 mM K$^+$. A 10-fold decrease in the K$^+$ concentration from 10 to 1 mM leads to an increase of about one log unit in Tl adsorption, in line with differences in pH-dependent adsorption in different background electrolytes, again pointing to a cation exchange mechanism as the dominant uptake process even at the lowest Tl concentrations.

The slope of the adsorption isotherm in 100 mM Na$^+$ electrolyte is below unity, indicating that there are at least two different adsorption sites with different capacities and affinities accessible to Tl$^+$. The increase in Tl$^+$ adsorption affinity with decreasing concentration and loading points to the presence of high affinity sites with limited adsorption capacity, where Na$^+$ is not strongly competitive. A very similar adsorption isotherm is observed in 5 mM Ca(NO$_3$)$_2$ (Figure 1C), in line with the known low affinity of alkaline earth cations for uptake at frayed edge sites.[34,49] The slope near unity of the adsorption isotherm in 1 and 10 mM K$^+$, on the other hand, indicates that K$^+$ effectively reduces high-affinity Tl$^+$ adsorption. A nearly identical adsorption isotherm as in 10 mM KNO$_3$ electrolyte was measured in 10 mM NH$_4$NO$_3$ electrolyte (Figure 1C), indicating that K$^+$ and NH$_4^+$ affect the extent of Tl$^+$ adsorption in a very similar way.

Cation Exchange Modeling. Cation exchange selectivity coefficients for Tl$^+$ exchange equilibria with respect to Na$^+$, K$^+$, NH$_4^+$, Ca^{2+}, were derived by fitting the five experimental adsorption isotherms (Figure 1BC) based on the site types and fractions from the generalized 3-site cation exchange model for Cs$^+$ onto illite. Preliminary fits indicated a very high negative

Table 1. Cation Exchange Selectivity Coefficients for Tl$^+$-Na$^+$, Tl$^+$-K$^+$, Tl$^+$-NH$_4^+$, and Tl$^+$-Ca^{2+} Exchange Refined from the Log K_d of Tl$^+$ in Homoionic Na-illite, K-illite, NH$_4$-illite, and Ca-illite Suspensions at near Neutral pH (Figure 2)[a]

site	FES	T2S	PS
site fractions[b]	0.25% of CEC	20% of CEC	79.75% of CEC
Tl-X Exchange Selectivity Coefficients Derived from Tl Isotherms			
log K_{Ca}^{Tl}	12.2 (0.1)	7.1 (0.1)	2.0 (0.2)
log K_{Na}^{Tl}	6.2 (0.1)	3.6 (0.1)	1.2 (0.1)
log K_{K}^{Tl}	2.9 (0.1)	0.5 (0.1)	0.5 (0.1)
log $K_{NH_4}^{Tl}$	2.8 (0.3)	1.4 (0.1)	0.3 (0.1)
Corresponding Exchange Selectivity Coefficients for Major Cations			
log K_{Na}^{Ca}	0.2 (0.1)	0.0 (0.1)	0.4 (0.2)
log $K_{Na}^{NH_4}$	3.4 (0.3)	2.1 (0.1)	0.9 (0.1)
log K_{Na}^{K}	3.3 (0.1)	3.0 (0.1)	0.7 (0.1)
Cs-X and Rb-X Exchange Selectivity Coefficients from Ref 35[c]			
log K_{Na}^{Cs}	7.0 (0.2)	3.6 (0.2)	1.6 (0.2)
log K_{Na}^{Rb}	5.5 (0.2)[c]	2.8 (0.2)[c]	1.4 (0.2)[c]
log K_{K}^{Cs}	4.6 (0.2)	1.5 (0.2)	0.5 (0.2)
log K_{K}^{Rb}	2.2 (0.2)	0.5 (0.2)	0.5 (0.2)

[a]Values in parentheses indicate numerical fit uncertainty. The selectivity coefficients for major cations were calculated from the Tl-X selectivity coefficients. Cs$^+$-X and Rb$^+$-X selectivity coefficients from Bradbury and Baeyens (2000)[35] are shown for comparison. [b]Site fractions from the generalized 3-site Cs$^+$ sorption model[35] were multiplied with the Tl-CEC of 0.260 eq/kg to obtain site concentrations. [c]Rb$^+$-Na$^+$ selectivity coefficients were obtained by remodeling Rb$^+$-Na$^+$ cation exchange date from ref 34 in the framework of the generalized 3-site sorption model as described for the corresponding Rb$^+$-K$^+$ selectivity coefficients in ref 35.

correlation between the Tl$^+$-K$^+$ selectivity coefficients on T2S and PS and the refined coefficients were nearly identical. Therefore, the two cation exchange coefficients were defined to be equal to reduce the associated parameter uncertainty. The optimized Tl-X selectivity coefficients are reported in Table 1, together with resulting cation exchange coefficients for major cations and for Cs$^+$ and Rb$^+$ from the generalized 3-site Cs$^+$ sorption model of Bradbury and Baeyens (2000).[35] The modeled log K_d values as a function of dissolved Tl concentrations are shown in Figure 2A–E, the modeled Tl adsorption isotherms in SI Figure S2.
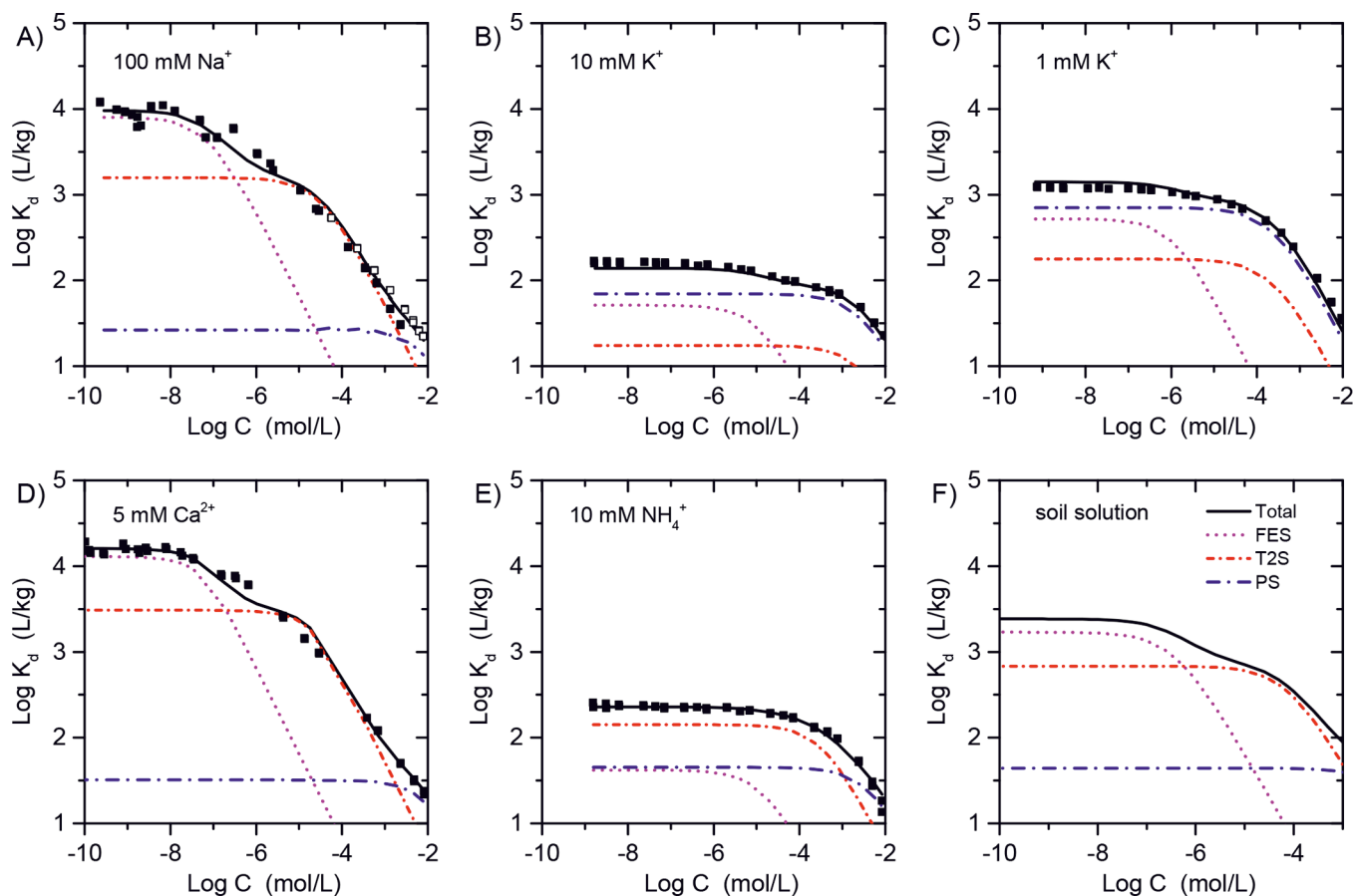
Figure 2. Log K_d (distribution coefficients) as a function of dissolved Tl^+ concentration for Tl^+ adsorption onto illite at near-neutral pH in (A) 100 mM NaCl (filled symbols) or $NaNO_3$, (unfilled symbols) (B) 10 mM KNO_3, (C) 1 mM KNO_3, (D) 5 mM $Ca(NO_3)_2$, and (E) 10 mM NH_4NO_3 (symbols). Model calculations (solid lines for total Tl^+ adsorption and broken colored lines for Tl^+ adsorption on FES, T2S, and PS) are based on parameters reported in Table 1. (F) Calculated log K_d for Tl^+ adsorption onto illite in arable soil porewater with typical concentrations of Ca^{2+} (2.00 mM), Mg^{2+} (0.46 mM), Na^+ (0.28 mM), K^+ (0.24 mM), and NH_4^+ (0.05 mM)[53] balanced by NO_3^- (see text for details).

Comparison of the Tl-Na or Tl-K exchange selectivity coefficients on FES and T2S with the Cs-Na and Rb-Na or Cs-K and Rb-K exchange coefficients of the generalized 3-site sorption model (Table 1) consistently indicate that, overall, Tl^+ adsorption onto illite exhibits an affinity between the affinities of Cs^+ and Rb^+. In Table 2, the Tl-X exchange coefficients on FES and T2S are compared to the effective ionic radii (for 12-fold coordination) and molar Gibbs hydration energies of the respective cation. The very high selectivity of Tl^+ with respect to Na^+ and Ca^{2+} on FES can be linked to the unsuitable ionic radii of Na^+ and Ca^{2+} and their (much) more negative hydration energies. With respect to the cations K^+, NH_4^+, Rb^+, and Cs^+, a consistent decrease in selectivity can be observed as a function of both increasing ionic radius and less negative hydration energy (higher tendency to dehydrate). The Tl^+ cation does not closely follow this trend with a cation exchange selectivity coefficient between Cs^+ and Rb^+, an ionic radius between NH_4^+ and Rb^+ and a hydration energy similar to K^+ (Table 2). This may be due to the fact that Tl is a post-transition metal in the boron group and not an alkali metal and that, consequently, the electronic configuration of the Tl^+ cation with a lone electron pair is markedly different from the cations K^+, Rb^+, and Cs^+.

From the Tl-X exchange coefficients, also the cation exchange selectivity coefficients of the major cations K^+, Ca^{2+}, and NH_4^+ versus Na^+ were derived (Table 1). For PS, it

Table 2. Comparison of the Effective Ionic Radii (for 12-Fold Coordination), Molar Gibbs Energies of Ion Hydration and Tl-X Selectivity Coefficients on FES and T2S for Different Cations X

cation X	ionic radius[a] (Å)	$\Delta G_{hydration}$[b] (kJ/mol)	$logK_X^{Tl}$ FES	$logK_X^{Tl}$ T2S
Ca^{2+}	1.34	−1505 (1205)	12.2	7.1
Na^+	1.39	−365 (65)	6.2	3.6
K^+	1.64	−295 (−5)	2.9	0.5
NH_4^+	1.67	−285 (−15)	2.8	1.4
Rb^+	1.72	−275 (−25)	0.7[c] (0.7)	0.8[c] (0)
Tl^+	1.70	−300		
Cs^+	1.88	−250 (−50)	−0.8[c] (−1.7)	0[c] (−1.0)

[a]Effective ionic radii for 12-fold coordinated cations from ref 3 except for NH_4^+ from ref 74. [b]Molar Gibbs energies of hydration from ref 75; Values in parentheses correspond to $\Delta G_{hydration, Tl} - \Delta G_{hydration, X}$. [c]$LogK_{Rb}^{Tl}$ and $logK_{Cs}^{Tl}$ calculated from $logK_{Na}^{Tl}$, $logK_{Na}^{Rb}$ and $logK_{Na}^{Cs}$ from Table 1. Values in parentheses were calculated from $logK_K^{Tl}$, $logK_K^{Rb}$, and $logK_K^{Cs}$ and are considered less reliable.

was found that the respective major cation exchange selectivity coefficients were close to K^+-Na^+, NH_4^+-Na^+, and Ca^{2+}-Na^+ selectivity coefficients reported for montmorillonite (log K_{Na}^K = 0.4 ± 0.2; log K_{Na}^{NH4} = 0.7 ± 0.1; log K_{Na}^{Ca} = 0.8 ± 0.4; derived from the compilation of cation exchange selectivity

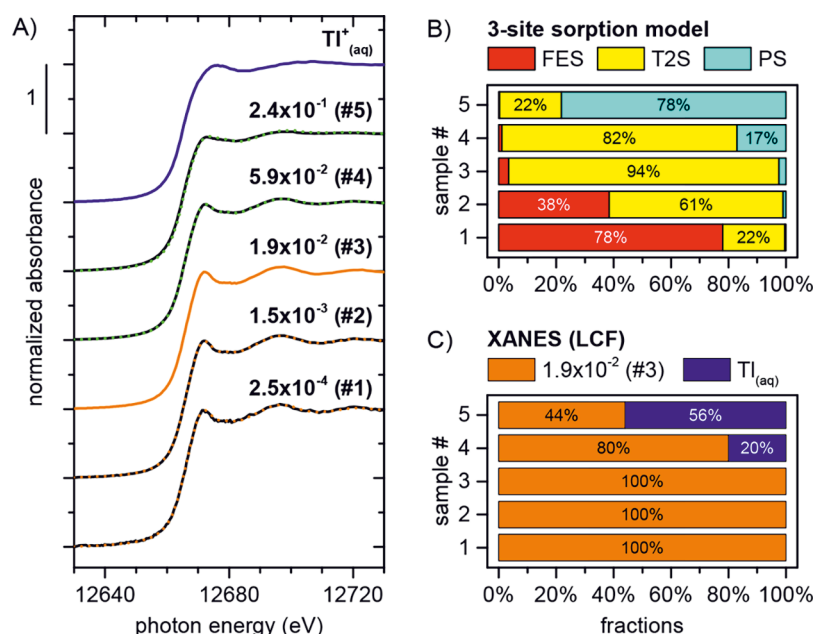**Figure 3.** (A) Tl L_{III}-edge XANES spectra of Na-IdP with Tl$^+$ loadings from 2.5×10^{-4} to 2.4×10^{-1} mol/kg (50 to 49 000 mg/kg) (solid orange line for sample #3, solid black lines for other samples) and of aqueous Tl$^+$ (10 mM TlNO$_3$; solid blue line). (B) Calculated distribution of Tl over sorption model sites. (C) Fractions of spectra of sample #3 and aqueous Tl$^+$ used to reproduce the sample spectra #1 to #5 (reconstructions shown as short dashed green or orange lines in panel A).

coefficients in ref 50), which may be taken as proxy for PS of illite. The major cation exchange coefficients for T2S and FES reflect a much stronger selectivity of K$^+$ and NH$_4^+$ than Na$^+$ and Ca^{2+} at the frayed edges of illite.

According to the model calculations, Tl uptake onto Na- and Ca-IdP is dominated by FES for Tl concentrations up to almost 10^{-7} M, and by T2S for concentrations up to nearly 10^{-3} M (Figure 2). In the 1 mM and especially the 10 mM K$^+$ electrolyte (K-IdP), in contrast, Tl$^+$ adsorption onto FES was substantially reduced, and Tl$^+$ adsorption to PS contributed significantly to total Tl uptake even at lowest Tl concentrations. For Tl$^+$ adsorption in 10 mM NH$_4^+$ electrolyte (NH$_4$-IdP), the fit returned site contributions that markedly varied from the 10 mM K$^+$ electrolyte, with a dominance of T2S over a wide Tl$^+$ concentration range. The discrepancy between the 10 mM K$^+$ and 10 mM NH$_4^+$ electrolytes in terms of adsorption site relevance may point to true differences in the impact of these ions on the preferential way of Tl$^+$ uptake, but may also just reflect that the respective fits were poorly constrained as two sites would have been sufficient to satisfactorily describe the respective log K_d curves.

Tl L_{III}-Edge XANES Spectra. Tl L_{III}-edge XANES spectra collected on Na-IdP with Tl loadings from 2.5×10^{-4} to 2.4×10^{-1} mol/kg Tl (samples #1 to #5; 50 to 49 000 mg/kg Tl) are shown in Figure 3, together with the modeled distribution of Tl over the three types of exchange sites considered in the model and results from the analysis of the sample spectra by spectral comparison or linear combination fitting (LCF). According to the model calculations, the Tl was mainly adsorbed to FES in sample #1 (2.5×10^{-4} mol/kg Tl), to T2S in sample #3 (1.9×10^{-2} mol/kg Tl), and to PS in sample #5 (2.4×10^{-1} mol/kg Tl) (Figure 3B).

From sample #1 (mainly Tl on FES) to sample #3 (mainly Tl on T2S), no marked spectral change was observed. Indeed, the spectra of samples #1 and #2 could be perfectly matched with the spectrum of sample #3 (Figure 3A), suggesting that Tl

coordination did not detectably vary over the respective range in Tl loading. In combination with the model calculations, this spectroscopic finding suggests that FES and T2S of the 3-site sorption model serve to describe the decreasing adsorption affinity of dehydrated Tl$^+$ bound at the frayed edges of illite platelets with increasing Tl loading, in line with the interpretation of these model sites in earlier work on the uptake of Cs$^+$ and Rb$^+$ by illite.[34,49]

From sample #3 (mainly Tl on T2S) to sample #5 (mainly Tl on PS), on the other hand, a clear shift in the spectra was observed. LCF analysis showed that spectra #4 and #5 could be adequately reproduced by linear combinations of the spectra of sample #3 and of hydrated aqueous Tl$^+$ (Figure 3AC). Assuming that the spectrum of sample #3 represents dehydrated Tl$^+$ adsorbed at the frayed edges of illite and the spectrum of aqueous Tl$^+$ represents hydrated Tl$^+$ adsorbed on planar sites, the spectral trend was in agreement with the adsorption model that indicated a transition from predominant Tl$^+$ adsorption at the frayed edges of illite in sample #3 to predominant adsorption of Tl$^+$ at planar sites in sample #5 (Figure 3B). The difference between the modeled fraction of Tl at PS and of LCF-derived fraction of hydrated Tl$^+$ in sample #5 may be due to various factors, including uncertainties in model calculations or the nonconsideration of the potential role of partially dehydrated adsorbed Tl$^+$ (on PS or at FES) in addition to fully dehydrated and fully hydrated Tl$^+$ (as inferred for Cs$^+$ uptake on clay minerals based on XAS results).[51,52]

Adsorption of Tl$^+$ onto Illite in Arable Soil Porewater. The adsorption of Tl$^+$ onto illite was modeled for typical concentrations of Ca^{2+}, Mg^{2+}, Na$^+$, K$^+$, and NH$_4^+$ in the porewater of arable soils (from ref 53 details in SI Table S2; Mg^{2+} assumed to exhibit the same cation exchange behavior as Ca^{2+}). For average cation concentrations, the modeled log K_d as a function of the dissolved Tl concentration is shown in Figure 2F, together with the contribution of the individual types of sites. The results show that Tl$^+$ adsorption onto illite
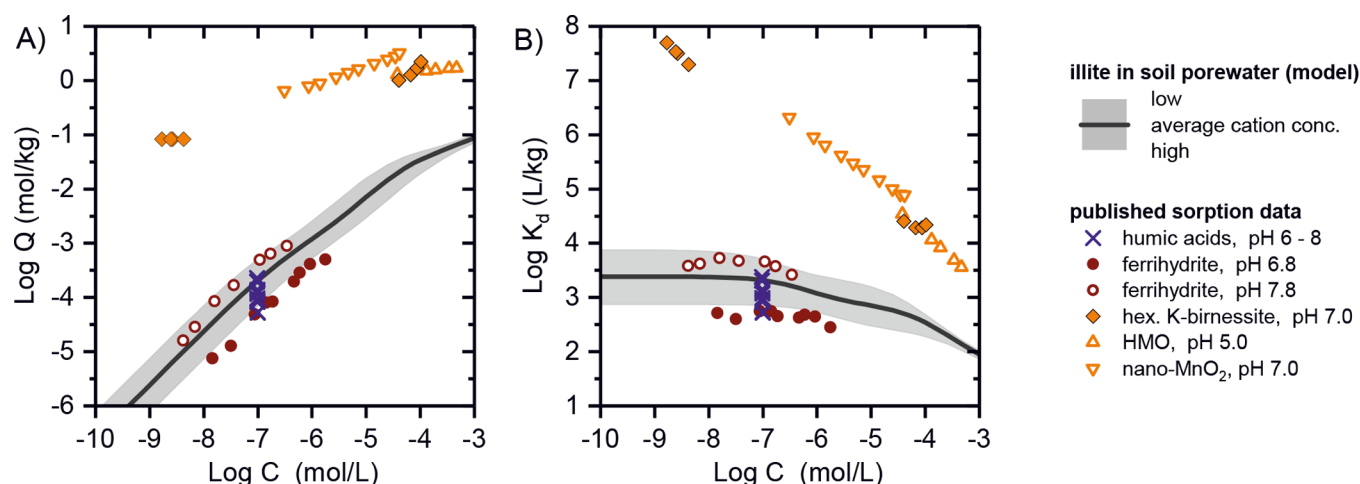
Figure 4. Modeled adsorption of Tl^+ onto illite in arable soil porewater (dark gray line; light gray area) shown as log adsorbed amounts (A) and log distribution coefficients (B) compared to published data (symbols) for Tl^+ adsorption onto two humic acids,[54] ferrihydrite[15] and three hexagonal birnessites.[55−57] Model calculations were performed with parameters from Table 1 for average (dark gray line) as well as low and high concentrations of Ca^{2+}, Mg^{2+}, Na^+, K^+, and NH_4^+ (light gray area) in arable soil porewater[53] (see text and SI Table S2 for details; average concentrations: 2.00 mM Ca^{2+}, 0.46 mM Mg^{2+}, 0.28 mM Na^+, 0.24 mM K^+, 0.05 mM NH_4^+). Published sorption data for two humic acids (in 100 mM $NaClO_4$),[54] ferrihydrite (in 10 mM NaCl),[15] hexagonal K-birnessite (in 110 mM KNO_3),[57] hydrous manganese oxide (HMO),[55] and nano-MnO_2 (in 2 mM MOPS)[56] (see SI for details on published sorption data).

in equilibrium with the soil solution was dominated by FES (and T2S) over environmentally relevant ranges in dissolved and adsorbed Tl^+, and that adsorption to PS was of minor importance (Figure 2F). This was also true if Tl^+ adsorption onto illite was modeled for the lower or upper bounds of common cation concentrations (not shown). Figure 4 shows the modeled adsorption of Tl^+ onto illite from arable soil porewater with average cation concentrations (thick black lines) as well as for lower and upper bounds of common concentration of Ca^{2+}, Mg^{2+}, Na^+, K^+, and NH_4^+ (light gray area). The calculations reveal that the log K_d (K_d in units of [L/kg]) for Tl^+ adsorption onto illite at dissolved concentrations $<10^{-7}$ M varies between 2.9 and 3.9. Further calculations with low Ca^{2+}, Mg^{2+} and Na^+ and high K^+ and NH_4^+ concentrations and vice versa (not shown) indicated that the trace Tl^+ adsorption isotherms strongly dependent on the concentrations of K^+ and NH_4^+ which compete for adsorption onto FES and T2S, but much less on the concentrations of Ca^{2+} and Mg^{2+}. However, these alkaline earth cations are relevant as they limit Tl^+ adsorption onto PS.

Comparison of Tl^+ Adsorption onto Illite and Other Adsorbents. In Figure 4, published data for Tl^+ adsorption onto humic acid,[54] ferrihydrite[15] and hexagonal birnessites[55−57] are compared to the predicted adsorption of Tl^+ onto illite in arable soil porewater. Noting that the sorption experiments with ferrihydrite and humic acids were performed in Na^+ electrolytes and do not reflect the effects of more competitively adsorbing cations, the comparison suggests that humic acids and Fe-oxides may also be important adsorbents for Tl in specific environments, for example, humic acids in forest topsoils for which enhanced levels of labile Tl have been attributed to Tl adsorption onto soil organic matter,[58] or ferrihydrite in environments affected by acid mine drainage.[15]

Consistent data for Tl^+ adsorption onto hexagonal birnessite, a synthetic proxy of biogenic Mn oxides,[59] was compiled from three studies[55−57] (Figure 4). The very strong uptake of Tl^+ by hexagonal birnessite at low dissolved Tl^+ concentrations has been attributed to oxidative Tl complex-

ation on vacancy sites in octahedral MnO_2 sheets (characteristic of hexagonal birnessite).[9,10] The strong decrease in the log K_d with increasing Tl loading points to a shift to less specific and probably nonoxidative sorption mechanisms after saturation of vacancy sites, as previously inferred from trends in Tl isotope fractionation.[57] The much higher log K_d of Tl bound to hexagonal birnessite than illite at low dissolved Tl^+ concentrations allows to rationalize the high enrichment of Tl in marine ferromanganese nodules relative to pelagic clays,[60] or the observation that addition of 0.5% (by weight) hexagonal birnessite to two soils spiked with 5 mg/kg Tl resulted in a depletion of the exchangeable Tl fraction and reduced Tl uptake by mustard, whereas addition of 1.5% illite did not show such an effect.[16] Conversely, the predominant association of Tl with illite in a geogenically Tl-rich soil has partly been attributed to high Tl loadings that exceeded the adsorption capacity of birnessite.[12] More generally, the role of hexagonal birnessite as an adsorbent for Tl in a specific environment, relative to illite and other adsorbents, may be constrained by various factors that are not reflected by the adsorption data shown in Figure 4, such as the abundance of the respective adsorbents, their chemical stability, and competitive cation uptake. For example, soils typically contain less than 1000 mg/kg Mn[61] and hexagonal birnessite may account for only a fraction of the soil Mn, whereas illite and other micaceous phyllosilicates often represent a major soil component. In addition, many trace elements that are typically more abundant than Tl such as Ba, Co, Ni, Cu, Zn, or Pb also strongly adsorb onto hexagonal birnessite[59,62,63] and may limit Tl uptake. Over time, biogenic hexagonal birnessite can also transform into Mn-oxides with lower adsorption capacity.[64] Finally, Mn-oxides are susceptible to reductive dissolution under anoxic conditions, which constrains their relevance and impact in periodically and permanently reducing environments.

Implications of Tl^+ Adsorption onto Illite and Other Micaceous Phyllosilicates. This study demonstrated that Tl^+ strongly adsorbs onto illite with an adsorption affinity between Rb^+ and Cs^+ and that Tl^+ uptake can be described

using a 3-site cation exchange model previously developed to describe the competitive adsorption of Cs^+, Rb^+, NH_4^+, and K^+ onto illite.[35] For Cs^+, high adsorption affinities at low loadings have also been documented for other micaceous phyllosilicates, most importantly (weathered) biotite and muscovite[33,65] and (hydroxy-interlayered) vermiculite,[29,66−68] but also illite-interstratified smectite.[69] Considering the results from this study, we postulate that Tl^+ will equally adsorb onto these minerals with a cation exchange selectivity between those of Rb^+ and Cs^+ (Table 2).

Studies with Cs^+ indicated that adsorption onto illite occurs within hours to days, but that desorption kinetics can be slow and that periods of months to even years may be necessary to reach desorption equilibrium, depending also on the concentrations of K^+ and NH_4^+ that may cause a collapse of the frayed edges and thereby inhibit desorption.[70−73] Assuming that Tl^+ behaves similarly, slow desorption kinetics may limit short-term Tl^+ release, for example during rapid water infiltration into soil during rain events, but equilibrium conditions can be assumed over longer reaction times and in less dynamic environments. Over longer periods of time, Tl^+ adsorbed at the FES of illite could also diffuse into the interlayer and become structurally fixed, as has been observed for Cs^+ and proposed for geogenic Tl in soils.[12,58] On the other hand, for a soil containing 12% illite and contaminated by the emissions of a cement plant, a high-fraction (∼70%) of the total soil Tl (3 mg/kg) was found to be present in exchangeable form and was also available for plant uptake, suggesting that Tl fixation in micaceous clay minerals over the time of soil contamination (or slow desorption kinetics) did not substantially limit Tl release.

As our results show, the amount of Tl^+ bound at the frayed edges of illite strongly depends on adsorption competition with K^+ and NH_4^+. Thus, processes that can lead to an increase of these cations in solution, such as fertilization of soils with K^+ or NH_4^+ or reduction of NO_3^- to NH_4^+ in flooded soils and sediments may strongly impact on Tl^+ solubility. The cation exchange model for Tl^+ adsorption onto illite derived in this study provides a solid basis to estimate such effects and, more generally, to assess the effect of Tl^+ adsorption onto illite on the retention and solubility of Tl in soils and sediments.

■ ASSOCIATED CONTENT

Ⓢ Supporting Information

The Supporting Information is available free of charge on the ACS Publications website at DOI: 10.1021/acs.est.7b04485.

> Time-resolved trace Tl adsorption onto Na-exchanged and K-exchanged IdP at different pH values, experimental and modeled adsorption isotherms for Tl^+ adsorption onto illite at near-neutral pH, experimental conditions of pH- and concentration-dependent adsorption experiments, derivation of common concentration of major cations in arable soil porewater and description of Tl^+ adsorption data for various adsorbents derived from the literature (PDF)

■ AUTHOR INFORMATION

Corresponding Author

*Phone: +41 58 765 54 70; fax: +41 58 765 58 02; e-mail: andreas.voegelin@eawag.ch.

ORCID Ⓞ

Andreas Voegelin: 0000-0003-2873-8966

Notes

The authors declare no competing financial interest.

■ REFERENCES

(1) Nriagu, J. O. *Thallium in the Environment*; John Wiley & Sons: New York, 1998; Vol. 29.

(2) John Peter, A. L.; Viraraghavan, T. Thallium: a review of public health and environmental concerns. *Environ. Int.* **2005**, *31*, 493−501.

(3) Shannon, R. D. Revised effective ionic radii and systematic studies of interatomic distances in halides and chalcogenides. *Acta Crystallogr., Sect. A: Cryst. Phys., Diffr., Theor. Gen. Crystallogr.* **1976**, *32*, 751−767.

(4) Jović, V. Thallium in rocks, soils, and plants: past progress and future needs. *Neues Jahrbuch für Mineralogie - Abhandlungen* **1993**, *166*, 43−52.

(5) Heinrichs, H.; Schulz-Dobrick, B.; Wedepohl, K. H. Terrestrial geochemistry of Cd, Bi, Tl, Zn and Rb. *Geochim. Cosmochim. Acta* **1980**, *44*, 1519−1533.

(6) Balič Žunić, T.; Moëlo, Y.; Lončar, Ž.; Micheelsen, H. Dorallcharite, $Tl_{0.8}K_{0.2}Fe_3(SO_4)_2(OH)_6$, a new member of the jarosite-alunite family. *Eur. J. Mineral.* **1994**, *6*, 255−263.

(7) Daiyan, C.; Guanxin, W.; Zhenxi, Z.; Yuming, C. Lanmuchangite, a new thallium (hydrous) sulphate from Lanmuchang, Guizhou Province, China. *Chin. J. Geochem.* **2003**, *22*, 185−192.

(8) Radtke, A. S.; Dickson, F. W.; Slack, J. F. Occurrence and formation of avicennite, Tl_2O_3, as a secondary mineral at the Carlin gold deposit, Nevada. *J. Res. U.S. Geol. Survey* **1978**, *6* (2), 241−246.

(9) Peacock, C. L.; Moon, E. M. Oxidative scavenging of thallium by birnessite: Explanation for thallium enrichment and stable isotope fractionation in marine ferromanganese precipitates. *Geochim. Cosmochim. Acta* **2012**, *84*, 297−313.

(10) Bidoglio, G.; Gibson, P. N.; O'Gorman, M.; Roberst, K. J. X-ray absorption spectroscopy investigation on surface redox transformations of thallium and chromium on colloidal mineral oxides. *Geochim. Cosmochim. Acta* **1993**, *57*, 2389−2394.

(11) Kabata-Pendias, A. *Trace Elements in Soils and Plants*. 4th ed.; CRC Press: Boca Raton, 2011.

(12) Voegelin, A.; Pfenninger, N.; Petrikis, J.; Majzlan, J.; Plötze, M.; Senn, A.-C.; Mangold, S.; Steininger, R.; Göttlicher, J. Thallium speciation and extractability in a thallium- and arsenic-rich soil developed from mineralized carbonate rock. *Environ. Sci. Technol.* **2015**, *49*, 5390−5398.

(13) Xiao, T.; Yang, F.; Li, S.; Zheng, B.; Ning, Z. Thallium pollution in China: A geo-environmental perspective. *Sci. Total Environ.* **2012**, *421−422*, 51−58.

(14) Kersten, M.; Xiao, T.; Kreissig, K.; Brett, A.; Coles, B. J.; Rehkämper, M. Tracing anthropogenic thallium in soil using stable isotope compositions. *Environ. Sci. Technol.* **2014**, *48*, 9030−9036.

(15) Casiot, C.; Egal, M.; Bruneel, O.; Verma, N.; Parmentier, M.; Elbaz-Poulichet, F. Predominance of aqueous Tl(I) species in the river system downstream from the abandoned Carnoulès mine (Southern France). *Environ. Sci. Technol.* **2011**, *45*, 2056−2064.

(16) Vaněk, A.; Komárek, M.; Vokurková, P.; Mihaljevic, M.; Šebek, O.; Panušková, G.; Chrastný, V.; Drábek, O. Effect of illite and birnessite on thallium retention and bioavailability in contaminated soils. *J. Hazard. Mater.* **2011**, *191*, 170−176.

(17) Cheam, V.; Garbai, G.; Lechner, J.; Rajkumar, J. Local impacts of coal mines and power plants across Canada. I. Thallium in waters and sediments. *Water Quality Research Journal of Canada* **2000**, *35* (4), 581−607.

(18) Campanella, B.; Onor, M.; D'Ulivo, A.; Giannecchini, R.; D'Orazio, M.; Petrini, R.; Bramanti, E. Human exposure to thallium through tap water: A study from Valdicastello Carducci and Pietrasanta (northern Tuscany, Italy). *Sci. Total Environ.* **2016**, *548−549*, 33−42.

(19) Xiao, T.; Boyle, D.; Guha, J.; Rouleau, A.; Hong, Y.; Zheng, B. Groundwater-related thallium transfer processes and their impacts on the ecosystem: southwest Guizhou Province, China. *Appl. Geochem.* **2003**, *18*, 675−691.

(20) Shaw, D. M. The geochemistry of thallium. *Geochim. Cosmochim. Acta* **1952**, *2*, 118−154.

(21) Jacobsen, A. R.; McBride, M. B.; Baveye, P.; Steenhuis, T. S. Environmental factors determining the trace-level sorption of silver and thallium to soils. *Sci. Total Environ.* **2005**, *345*, 191−205.

(22) Matthews, A. D.; Riley, J. P. The occurrence of thallium in sea water and marine sediments. *Chem. Geol.* **1970**, *6*, 149−152.

(23) Lehn, H.; Schoer, J. Thallium-transfer from soils to plants: Correlation between chemical form and plant uptake. *Plant Soil* **1987**, *97*, 253−265.

(24) Tremel, A.; Masson, P.; Sterckeman, T.; Baize, D.; Mench, M. Thallium in French agrosystems - I. Thallium contents in arable soils. *Environ. Pollut.* **1997**, *95* (3), 293−302.

(25) Meunier, A.; Velde, B. *Illite*; Springer-Verlag: Berlin, Heidelberg, 2004; p 286.

(26) Fuller, A. J.; Shaw, S.; Ward, M. B.; Haigh, S. J.; Mosselmans, J. F. W.; Peacock, C. L.; Stackhouse, S.; Dent, A. J.; Trivedi, D.; Burke, I. T. Caesium incorporation and retention in illite interlayers. *Appl. Clay Sci.* **2015**, *108*, 128−134.

(27) Jackson, M. *Weathering of Primary and Secondary Minerals in Soils* **1968**, *4*, 281−292.

(28) Bolt, G. H.; Sumner, M. E.; Kamphorst, A. A study of the equilibria between three categories of potassium in an illitic soil. *Soil Sci. Soc. Am. Proc.* **1963**, *27*, 294−299.

(29) Sawhney, B. L., Selective sorption and fixation of cations by clay minerals: A review. *Clays Clay Miner.* **1972**, *20*, (93−100).9310.1346/CCMN.1972.0200208

(30) Komarneni, S. Cesium sorption by clay-minerals and shales at elevated-temperatures. *J. Inorg. Nucl. Chem.* **1979**, *41* (3), 397−400.

(31) Komarneni, S.; Roy, D. M. Shale as a radioactive-waste repository - Importance of vermiculite. *J. Inorg. Nucl. Chem.* **1979**, *41* (12), 1793−1796.

(32) Tamura, T.; Jacobs, D. G. Structural implications in cesium sorption. *Health Phys.* **1960**, *2* (4), 391−398.

(33) Zachara, J. M.; Smith, S. C.; Liu, C.; McKinley, J. P.; Serne, R. J.; Gassmann, P. L. Sorption of Cs+ to micaceous subsurface sediments from the Hanford site, USA. *Geochim. Cosmochim. Acta* **2002**, *66*, 193−211.

(34) Brouwer, E.; Baeyens, B.; Maes, A.; Cremers, A. Cesium and rubidium ion equilibria in illite clay. *J. Phys. Chem.* **1983**, *87*, 1213−1219.

(35) Bradbury, M. H.; Baeyens, B. A generalised model for the concentration dependent uptake of caesium by argillaceous rocks. *J. Contam. Hydrol.* **2000**, *42*, 141−163.

(36) Jacobson, A. R.; McBride, M. B.; Baveye, P.; Steenhuis, T. S. Environmental factors determining the trace-level sorption of silver and thallium to soils. *Sci. Total Environ.* **2005**, *345*, 191−205.

(37) Bradbury, M. H.; Baeyens, B. Sorption modelling on illite. Part I: Titration measurements and the sorption of Ni, Co, Eu and Sn. *Geochim. Cosmochim. Acta* **2009**, *73* (4), 990−1003.

(38) Bradbury, M. H.; Baeyens, B. Sorption modelling on illite. Part II: Actinide sorption and linear free energy relationships. *Geochim. Cosmochim. Acta* **2009**, *73* (4), 1004−1013.

(39) Schnurr, A.; Marsac, R.; Rabung, T.; Lutzenkirchen, J.; Geckeis, H. Sorption of Cm(III) and Eu(III) onto clay minerals under saline conditions: Batch adsorption, laser-fluorescence spectroscopy and modeling. *Geochim. Cosmochim. Acta* **2015**, *151*, 192−202.

(40) Poinssot, C.; Baeyens, B.; Bradbury, M. H. Experimental and modelling studies of caesium sorption on illite. *Geochim. Cosmochim. Acta* **1999**, *63* (19/20), 3217−3227.

(41) van Olphen, H.; Fripiat, J. J. *Data Handbook for Clay Materials and Other Non-Metallic Minerals*; Pergamon: Oxford a.o., 1979; p 346.

(42) Baeyens, B.; Bradbury, M. H. Cation exchange capacity measurements on illite using the sodium and cesium isotope dilution technique: Effects of the index cation, electrolyte concentration and competition: Modeling. *Clays Clay Miner.* **2004**, *52* (4), 421−431.

(43) Gaines, G. L. J.; Thomas, H. C. Adsorption studies on clay minerals. II: A formulation of the thermodynamics of exchange adsorption. *J. Chem. Phys.* **1953**, *21*, 714−718.

(44) Parkhurst, D. L.; Appelo, C. A. J. *User's guide to PHREEQC (Version 2)—A Computer Program for Speciation, Batch-Reaction, One-Dimensional Transport, And Inverse Geochemical Calculations*, 99-4259; U.S. Geological Survey: Denver, CO, 1999; p 312.

(45) Kinniburgh, D. G.; Cooper, D. M. PhreePlot: Creating graphical output with PHREEQC. http://www.phreeplot.org.

(46) Ravel, B.; Newville, M. ATHENA, ARTEMIS, HEPHAESTUS: data analysis for X-ray absorption spectroscopy using IFEFFIT. *J. Synchrotron Radiat.* **2005**, *12*, 537−541.

(47) Bradbury, M. H.; Baeyens, B.; Geckeis, H.; Rabung, T. Sorption of Eu(III)/Cm(III) on Ca-montmorillonite and Na-illite. Part 2: Surface complexation modelling. *Geochim. Cosmochim. Acta* **2005**, *69* (23), 5403−5412.

(48) Köhler, S. J.; Dufaud, F.; Oelkers, E. H. An experimental study of illite dissolution kinetics as a function of pH from 1.4 to 12.4 and temperature from 5 to 50°C. *Geochim. Cosmochim. Acta* **2003**, *67*, 3583−3594.

(49) Benedicto, A.; Missana, T.; Fernández, A. M. Interlayer collapse affects on cesium adsorption onto illite. *Environ. Sci. Technol.* **2014**, *48*, 4909−4915.

(50) Bruggenwert, M. G. M.; Kamphorst, A., Survey of experimental information on cation exchange in soil systems. In *Soil Chemistry: B. Physico-Chemical Models*; Bolt, G. H., Ed.; Elsevier: Amsterdam, 1979; pp 141−203.

(51) Bostick, B. C.; Vairavamurthy, M. A.; Karthikeyan, K. G.; Chorover, J. Cesium adsorption on clay minerals: an EXAFS spectroscopic investigation. *Environ. Sci. Technol.* **2002**, *36* (12), 2670−2676.

(52) Kemner, K. M.; Hunter, D. B.; Bertsch, P. M.; Kirkland, J. P.; Elam, W. T. Determination of site specific binding environments of surface sorbed cesium on clay minerals by Cs-EXAFS. *J. Phys. IV* **1997**, *7* (C2), 777−779.

(53) Blume, H. P.; Scheffer, F.; Schachtschabel, P. *Scheffer/Schachtschabel Soil Science*; Springer Verlag: Berlin, Heidelberg, 2016; p 618.

(54) Liu, J.; Lippold, H.; Wang, J.; Lippmann-Pipke, J.; Chen, Y. Sorption of thallium(I) onto geological materials: Influence of pH and humic matter. *Chemosphere* **2011**, *82*, 866−871.

(55) Wan, S.; Ma, M.; Lv, L.; Qian, L.; Xiu, S.; Xue, Y.; Ma, Z. Selective capture of thallium(I) ion from aqueous solutions by amorphous hydrous manganese dioxide. *Chem. Eng. J.* **2014**, *239*, 200−206.

(56) Huangfu, X.; Jiang, J.; Lu, X.; Wang, Y.; Liu, Y.; Pang, S.-Y.; Cheng, H.; Zhang, X. H.; Ma, J. Adsorption and oxidation of thallium(I) by a nanosized manganese dioxide. *Water, Air, Soil Pollut.* **2015**, *226* (2272), 1−9.

(57) Nielsen, S. G.; Wasylenki, L. E.; Rehkämper, M.; Peacock, C. L.; Xue, Z.; Moon, E. M. Towards an understanding of thallium isotope fractionation during adsorption to manganese oxide. *Geochim. Cosmochim. Acta* **2013**, *117*, 252−265.

(58) Vaněk, A.; Chrastný, V.; Mihaljevic, M.; Drahota, P.; Grygar, T.; Komárek, M. Lithogenic thallium behavior in soils with different land use. *J. Geochem. Explor.* **2009**, *102*, 7−12.

(59) Tebo, B. M.; Bargar, J. R.; Clement, B. G.; Dick, G. J.; Murray, K. J.; Parker, D.; Verity, R.; Webb, S. M. Biogenic manganese oxides:

Properties and mechanisms of formation. *Annu. Rev. Earth Planet. Sci.* **2004**, *32*, 287−328.

(60) Flegal, A. R.; Sanudo-Wilhelmy, S. Particulate thallium fluxes in the Northeast Pacific. *Mar. Chem.* **1989**, *28*, 61−75.

(61) Salminen, R. *Geochemical Atlas of Europe. Part 1: Background Information, Methodology and Maps*; Geological Survey of Finland: Espoo, 2005; p 526.

(62) Manceau, A.; Lanson, B.; Drits, V. A. Structure of heavy metal sorbed birnessite. Part III: Results from powder and polarized extended X-ray absorption fine structure spectroscopy. *Geochim. Cosmochim. Acta* **2002**, *66* (15), 2639−2663.

(63) Peacock, C. L.; Sherman, D. M. Sorption of Ni by birnessite: Equilibrium controls on Ni in seawater. *Chem. Geol.* **2007**, *238*, 94−106.

(64) Atkins, A. L.; Shaw, S.; Peacock, C. L. Nucleation and growth of todorokite from birnessite: Implications for trace-metal cycling in marine sediments. *Geochim. Cosmochim. Acta* **2014**, *144*, 109−125.

(65) Mukai, H.; Hirose, A.; Motai, S.; Kikuchi, R.; Tanoi, K.; Nakanishi, T. M.; Yaita, T.; Kogure, T. Cesium adsorption/desorption behavior of clay minerals considering actual contamination conditions in Fukushima. *Sci. Rep.* **2016**, *6* (6:21543), 1−7.

(66) Zaunbrecher, L. K.; Cygan, R. T.; Elliott, W. C. Molecular models of cesium and rubidium adsorption on weathered micaceous minerals. *J. Phys. Chem. A* **2015**, *119*, 5691−5700.

(67) Zaunbrecher, L. K.; Elliott, W. C.; Wampler, J. M.; Perdrial, N.; Kaplan, D. I. Enrichment of cesium and rubidium in weathered micaceous materials at the Savannah river site, South Carolina. *Environ. Sci. Technol.* **2015**, *49*, 4226−4234.

(68) Fan, Q. H.; Tanaka, M.; Tanaka, K.; Sakaguchi, A.; Takahashi, Y. An EXAFS study on the effects of natural organic matter and the expandability of clay minerals on cesium adsorption and mobility. *Geochim. Cosmochim. Acta* **2014**, *135*, 49−65.

(69) Missana, T.; Benedicto, A.; García-Gutiérrez, M.; Alonso, U. Modeling cesium retention onto Na-, K- and Ca-smectite: Effects of ionic strength, exchange and competing cations on the determination of selectivity coefficients. *Geochim. Cosmochim. Acta* **2014**, *128*, 266−277.

(70) Durrant, C. B.; Begg, J. D.; Kersting, A. B.; Zavarin, M. Cesium sorption reversibility and kinetics on illite, montmorillonite, and kaolinite. *Sci. Total Environ.* **2018**, *610−611*, 511−520.

(71) de Koning, A.; Comans, R. N. J. Reversibility of radiocaesium sorption on illite. *Geochim. Cosmochim. Acta* **2004**, *68*, 2815−2823.

(72) Comans, R. N. J.; Haller, M.; de Peter, P. Sorption of cesium on illite: Non-equilibrium behaviour and reversibility. *Geochim. Cosmochim. Acta* **1991**, *55*, 433−440.

(73) Comans, R. N. J., Kinetics and reversibility of radiocesium sorption on illite and sediments containing illite. In *Mineral-Water Interfacial Reactions: Kinetics and Mechanisms*; Sparks, D. L.; Grundl, T. J., Eds.; ACS: 1999.

(74) Sidey, V. On the effective ionic radii for ammonium. *Acta Crystallogr., Sect. B: Struct. Sci., Cryst. Eng. Mater.* **2016**, *72*, 626−633.

(75) Marcus, Y. Thermodynamics of solvation of ions. 5. Gibbs free-energy of hydration at 298.15 K. *J. Chem. Soc., Faraday Trans.* **1991**, *87* (18), 2995−2999.